

VideoMat: Extracting PBR Materials from Video Diffusion Models

JACOB MUNKBERG, NVIDIA, Sweden

ZIAN WANG, NVIDIA, University of Toronto, Vector Institute, Canada

RUOFAN LIANG, NVIDIA, University of Toronto, Vector Institute, Canada

TIANCHANG SHEN, NVIDIA, University of Toronto, Vector Institute, Canada

JON HASSELGREN, NVIDIA, Sweden



Fig. 1. Given a 3D model and a prompt, we extract high quality PBR materials from finetuned video diffusion models.

We leverage finetuned video diffusion models, intrinsic decomposition of videos, and physically-based differentiable rendering to generate high quality materials for 3D models given a text prompt or a single image. We condition a video diffusion model to respect the input geometry and lighting condition. This model produces multiple views of a given 3D model with coherent material properties. Secondly, we use a recent model to extract intrinsics (base color, roughness, metallic) from the generated video. Finally, we use the intrinsics alongside the generated video in a differentiable path tracer to robustly extract PBR materials directly compatible with common content creation tools.

CCS Concepts: • **Computing methodologies** → *Appearance and texture representations*; Ray tracing; Reflectance modeling.

Additional Key Words and Phrases: Text-to-material, Material generation, Differentiable Rendering, Video diffusion models

1 INTRODUCTION

DreamFusion [Poole et al. 2022] kickstarted a new research field of leveraging diffusion models to generate 3D models from text prompts. Most approaches extract data from image diffusion models through differentiable rendering, typically using neural radiance fields [Mildenhall et al. 2020] (NeRFs) or 3D Gaussian splats (3DGS) [Kerbl et al. 2023]. While results look impressive, e.g., for novel view synthesis, extracting materials for physically-based rendering (PBR) [Burley 2012; Walter et al. 2007] remains challenging. The lack of view-consistency in image diffusion models typically introduces blur and washes out material details. This is particularly obvious when extracting parameters for PBR materials models which relies on consistency of specular reflections. Furthermore,

multi-view optimization in a surface-based renderer which disentangles materials and lighting, e.g., a physically-based path tracer, is substantially more challenging than optimizing the volumetric approaches of NeRFs and 3DGS which bake lighting and material in common appearance representations.

Video diffusion models are beneficial for extracting spatially varying and specular materials. They far exceed image diffusion models in handling specular highlights and provide increased view consistency. This greatly helps when extracting material parameters and for intrinsic decomposition [Liang et al. 2025].

We present a method for text-to-material extraction based on video diffusion models. Our method starts from a known 3D geometry and a text prompt describing the desired material. We condition a diffusion model on G-buffer guides (normals, uniform shading), similar to previous work [Deng et al. 2024; Zhang et al. 2024a], which we extend to the video domain. By finetuning a recent video model, Cosmos [2025], with these conditions, we generate video sequences of known 3D objects with synthesized materials and controlled lighting. We then apply the inverse rendering pipeline of DiffusionRenderer [Liang et al. 2025] to extract *albedo*, *roughness*, and *metallic* material maps from the generated video. Finally, materials are baked to texture maps through a multi-view optimization using a differentiable path tracer regularized on the guides extracted by DiffusionRenderer.

As shown in Figure 1, we produce spatially varying, detailed materials that are robust to varying lighting conditions. In comparison to related work [Fang et al. 2024; Youwang et al. 2024; Zhang et al. 2024a], we show higher quality results and improved separation of lighting and materials.

Authors' addresses: Jacob Munkberg, NVIDIA, Sweden; Zian Wang, NVIDIA, and University of Toronto, and Vector Institute, Canada; Ruofan Liang, NVIDIA, and University of Toronto, and Vector Institute, Canada; Tianchang Shen, NVIDIA, and University of Toronto, and Vector Institute, Canada; Jon Hasselgren, NVIDIA, Sweden.

2 RELATED WORK

2.1 Video Diffusion Models

Diffusion models construct a Markov chain that gradually adds random noise to data through a sequence of diffusion steps. They are trained to reverse this process, enabling sample generation by a denoising process starting from Gaussian noise. Several diffusion-based generative models have been developed based on similar principles [Dhariwal and Nichol 2021; Ho et al. 2020; Sohl-Dickstein et al. 2015]. Recently, video diffusion models [Blattmann et al. 2023a,b; Hong et al. 2023; NVIDIA 2025; Yang et al. 2024b] extend image-based diffusion approaches to the temporal domain, enabling video generation from inputs such as text or an initial frame. In this work, we build upon the Cosmos [2025] video diffusion model.

2.2 Differentiable Rendering

Fuzzy scene representations such as NeRFs [Mildenhall et al. 2020] and Gaussian splatting [Kerbl et al. 2023] are commonly used in optimization setups, and generate impressive novel-view synthesis results. However, disentangling materials and lighting is non-trivial. In this paper, we focus on surface geometry with PBR materials [Burlley 2012]. Previous work include differentiable rasterization [Laine et al. 2020], which has low run-time cost and has been successfully applied to photogrammetry [Munkberg et al. 2022]. Differentiable path tracing [Jakob et al. 2022; Zhang et al. 2020] approaches are considerably more costly, and introduce Monte-Carlo noise in the training process, which can make gradient-based optimization more challenging. However, path tracing accurately simulates global illumination effects, and has higher potential reconstruction quality. In this work we use a custom path tracer similar to publicly available solutions [Jakob et al. 2022] but with inline support for querying a hashgrid [Müller et al. 2022] representation in the ray tracing loop.

2.3 Material Extraction from Diffusion Models

DreamFusion [Poole et al. 2022] introduces a *score distillation sampling* (SDS) loss, and generates 3D assets from pre-trained text-to-image diffusion models. This approach has since been refined [Wang et al. 2023; Zhu and Zhuang 2023] and integrated in many text-to-3D pipelines [Chen et al. 2023a; Wang et al. 2023] to extract PBR materials. Paint-it [Youwang et al. 2024] proposes representing material texture maps with randomly initialized convolution-based neural kernels. This regularizes the optimization landscape, improving material quality.

TextureDreamer [Yeh et al. 2024] finetunes the diffusion model using Dreambooth [Ruiz et al. 2022] with a few images of a 3D object, and uses *variational score distillation* [Wang et al. 2023] to optimize the material maps. DreamMat [Zhang et al. 2024a] and FlashTex [Deng et al. 2024] improve on light and material disentanglement by finetuning image diffusion models to condition on geometry and lighting, allowing for optimization over many known lighting conditions. Various hybrid approaches combine SDS with inpainting, or coarse-to-fine texture refinement [Chen et al. 2023b; Richardson et al. 2023; Zeng et al. 2024a].

A common limitation for most image models is lack of view consistency, which may show up as blur in the extracted textures. SV3D [Voleti et al. 2024] and Hi3D [Yang et al. 2024a] improve on

this aspect by finetuning video models for object rotations, and extract 3D models from the generated views. However, these approaches have limited resolution and do not provide PBR materials. Trellis [Xiang et al. 2024] and TEXGen [Yu et al. 2024] avoid the view consistency problem altogether by having the diffusion model operate directly in 3D space [Xiang et al. 2024] and texture space [Yu et al. 2024] respectively. These methods show great promise, but they are limited by training on relatively small, synthetic datasets of 3D assets.

MaPa [Zhang et al. 2024b], MatAtlas [Ceylan et al. 2024], and Make-it-Real [Fang et al. 2024] start from a database of known high-quality materials, and learn to project the input (image or text) onto the known representation. MaPa relies on material graphs and optimize parameters of known graphs, while Make-it-Real uses a database of PBR-textures, and MatAtlas a database of procedural materials. These methods are limited by the expressiveness of their material databases, but benefit from much improved regularization.

There are also several approaches for 3D asset creation through large-scale generative models. CLAY [Zhang et al. 2024c] generates 3D geometry and materials from text and image inputs. Their material generation model uses a finetuned multi-view image diffusion model [Shi et al. 2023] conditioned on normal maps. The material model generates four canonical views of the PBR texture maps (albedo, roughness, metallic), which are then projected into texture space. 3DTopia-XL [Chen et al. 2024] proposes a novel 3D representation, which encodes the 3D shape, textures, and materials in volumetric primitive anchored to the surface of the object. Their denoising process jointly generates shape and PBR materials. In concurrent work, MCMat [Zhu et al. 2024] leverages Diffusion Transformers (DiT) to extract multi-view images of PBR material maps, combined with a second DiT to enhance details in UV space.

Another related line of research is intrinsic decomposition of images. IntrinsicAnything [Xi et al. 2024] decomposes images into diffuse and specular components, and leverages these components as priors using physically-based inverse rendering to extract material maps. MaterialFusion [Litman et al. 2025] introduces a 2D diffusion model prior to help estimate material parameters in an multi-view reconstruction pipeline. RGB \leftrightarrow X [Zeng et al. 2024b] shows both intrinsic decomposition into G-buffers and neural rendering from G-buffers using diffusion models. DiffusionRenderer [Liang et al. 2025] extends RGB \leftrightarrow X to videos, and also support relighting. NeuralGaffer [Jin et al. 2024] and DiLightNet [Zeng et al. 2024c] leverage diffusion models for relighting single views. IllumiNerf [Zhao et al. 2024] relights each view in a multi-view dataset, then reconstructs a NeRF model with these relit images.

In concurrent work, IntrinsicX [Kocsis et al. 2025] combines intrinsic predictions for PBR G-buffers for a single view from text (using image diffusion models) with a rendering loss. Our approach is related, in that we combine intrinsic predictions and differentiable rendering. However, our goal is extracting PBR maps in *texture space*, which requires consistent predictions from many views. To that end, we leverage video diffusion models for view-consistent multi-view predictions and a more accurate renderer and lighting model in our rendering loss.

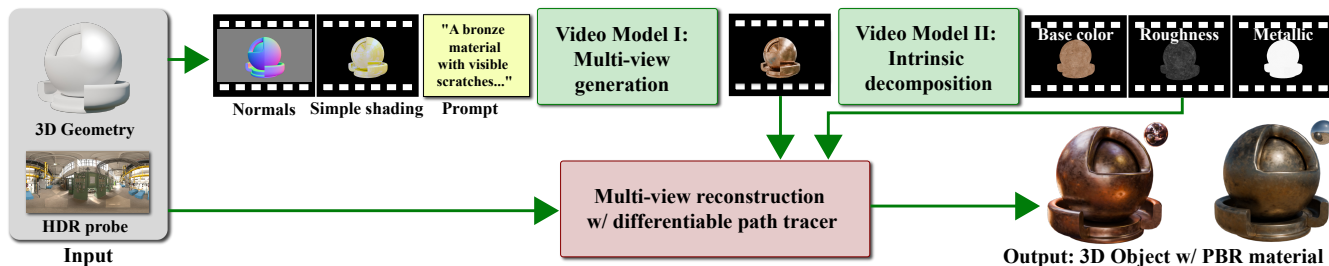


Fig. 2. Our method starts from a known 3D model and an HDR environment map. We first render videos of normal maps and three simple uniform shading conditions (diffuse, semi-specular, fully specular) lit with the provided probe. Next, these conditions, together with a text prompt, are passed to our finetuned video model, which generates a coherent video of the object with a novel material, while respecting the given lighting condition. We then pass this video into a second video model, which performs intrinsic decomposition, and generate per-frame G-buffers for the material properties. Finally, the output from the two video models, alongside the given geometry and lighting, are passed to a differentiable path tracer, which performs multi-view reconstruction to extract high quality PBR materials from the generated views.

3 METHOD

Our pipeline, as shown in Figure 2, combines two video models with a differentiable renderer to extract PBR material textures. We assume a given 3D model with a unique texture parametrization, and a lighting condition specified by an HDR light probe. We first generate frames for a 360° orbit from a video model, conditioned on geometry and lighting. Next, we run multi-view reconstruction from the generated views using differentiable rendering to extract the material maps. To regularize the reconstruction process, we leverage image intrinsics extracted from the generated video using a second video model. Below, we describe each step in detail.

3.1 Video Model I: Multi-view generation

In a first step, we generate videos of a 360° camera revolution around the 3D model, based on a text prompt describing the object’s material. We finetune a recent Diffusion Transformer (DiT) video model, Cosmos [2025], with additional conditions to respect the lighting and input geometry. We use the Cosmos-1.0-Diffusion-7BVideo2World¹ base model which operates in a latent space with 8× compression in the spatial and temporal domain. Encoding and decoding to and from latent space is done by the pretrained VAE Cosmos-1.0-Tokenizer-CV8x8x8. The base model supports text- and image guided video generation at a resolution of 1280×704 pixels and 121 frames.

Similar to DreamMat [Zhang et al. 2024a] and FlashTex [Deng et al. 2024] we condition the diffusion models with intrinsic guides: normals in camera space, and a *simple shading* guide which provides scene lighting information. The shading guide is rendered using three uniform materials with constant albedo, $k_d = 0.7$, roughness, $r = \{1, 0.5, 0\}$ and metallic, $m = \{0, 0.5, 1\}$, as shown in Figure 3. We compress the three shading guides into a single RGB-image by encoding the luminance of each image as a separate channel and provide these conditions per-frame.

We increase the input feature count of the input embedding layer of the diffusion model to account for our additional inputs (normals and simple shading), encoded into latent space using the frozen Cosmos tokenizer. We concatenate the encoded features with the noisy

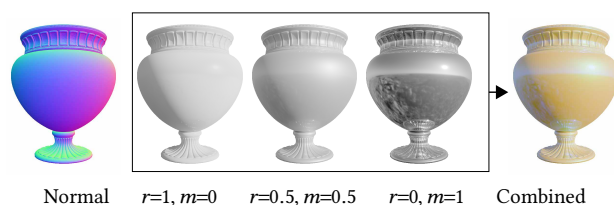


Fig. 3. We condition the video model with normal maps and three shading conditions, all with a uniform base color $k_d = (0.7, 0.7, 0.7)$ and varying roughness (r) and metallic (m) parameters. The shading conditions are combined into an RGB image.

video in latent space along the channel dimension, and finetune the embedding layer and all DiT layers using a custom dataset for 10k iterations on 64 GPUs. We use the the denoising score matching loss from Cosmos [2025] unmodified.

Our dataset consists of 40k videos of object-centric 360° orbits of 3D models from Objaverse [Deitke et al. 2023], BlenderVault [Litman et al. 2025], ShaderBalls [Mazzone and Rydalch 2023] (50 materials), ABO [Collins et al. 2022], and HSSD [Khanna* et al. 2023]. For each object, we render a video with 121 frames at a resolution of 1280×704 using a path tracer with three bounces. For lighting, we use a randomly selected probe from 670 HDR maps from Poly Haven [Zaal and et al. 2024]. We also render the intrinsic normal and simple shading guides from Figure 3. Video captions are automatically generated using the CogVLM2 [Hong et al. 2024] model. Since our videos are cyclical, we augment the dataset by randomly reversing the video, and randomly offsetting the video start frame on each training iteration.

3.2 Video Model II: Intrinsic Decomposition

To extract intrinsic channels—base color, roughness, and metallic maps—from the generated video, we re-implement the inverse renderer from DiffusionRenderer [Liang et al. 2025]. The inverse renderer is a video diffusion model that estimates material attributes conditioned on the input video. The same model is used to generate all material attributes. It generates one material map at a time, and

¹<https://github.com/NVIDIA/Cosmos>

uses optimizable domain embeddings to specify the target attributes to generate.

We finetuned the inverse rendering model from the Cosmos [2025] base model Cosmos-1.0-Diffusion-7BVideo2World, which provides higher quality results than the SVD-based [Blattmann et al. 2023a] version from the DiffusionRenderer paper. We follow the training pipeline from DiffusionRenderer closely, and finetune the base model using 150k videos with objects from Objaverse [Deitke et al. 2023].

3.3 Differentiable Rendering

To extract materials from the generated videos, we run multi-view reconstruction with a differentiable path tracer. Our renderer is similar to publicly available solutions, e.g., Mitsuba3 [Jakob et al. 2022], but with added support for querying a hash grid+MLP [Müller et al. 2022] representation inline in the ray tracing loop. We leverage this representation as a multi-scale material representation. As noted in methods using SDS loss [Chen et al. 2023a; Wang et al. 2023], the hierarchical hash grid+MLP representation is more robust to errors and noisy loss functions than 2D texture maps. By inlining the hash grid+MLP evaluation in the path tracer, we avoid 1) the render-PyTorch roundtrip for each evaluation and 2) logic to gather a large batch of shading requests for the PyTorch evaluations to be efficient. After optimization, we sample out the hash grid into standard 2D texture maps. We leverage CUDA WMMA instructions for efficient evaluation of the MLP linear layers, Slang [Bangaru et al. 2023] shaders (for autodiff) and GPU-accelerated OptiX [Parker et al. 2010] ray tracing kernels.

The differentiable renderer takes a 3D model and HDR probe, alongside camera poses and 121 frames from 1) the generated video (Video Model I) and 2) intrinsics (Video Model II). We run multi-view reconstruction to optimize the material maps for 1k iterations with a batch size of eight, using 1-3 bounces, 128 spp in the forward pass and 4 spp in the backward pass.

Shading model. Our goal is all-frequency lighting including shadows, reflections, and indirect illumination. The outgoing radiance $L(\omega_o)$ in direction ω_o can be expressed using the rendering equation [Kajiya 1986]:

$$L(\omega_o) = \int_{\Omega} L_i(\omega_i) f(\omega_i, \omega_o) (\omega_i \cdot \mathbf{n}) d\omega_i. \quad (1)$$

This is an integral of the product of the incident radiance, $L_i(\omega_i)$ from direction ω_i and the BSDF $f(\omega_i, \omega_o)$. The integration domain is the hemisphere Ω around the surface intersection normal, \mathbf{n} .

We use the physically-based (PBR) material model from Disney [Burley 2012] which combines a Lambertian term and a Cook-Torrance microfacet specular shading model [Cook and Torrance 1982]:

$$f(\omega_i, \omega_o) = \frac{DGF}{4(\omega_o \cdot \mathbf{n})(\omega_i \cdot \mathbf{n})}, \quad (2)$$

where D , G and F are functions representing the GGX [Walter et al. 2007] normal distribution (NDF), geometric attenuation and Fresnel term, respectively. This BSDF is parameterized with an RGB base color, c_{base} , and scalar roughness, r , and metallic, m , values at each shading point. The specular lobe is described by the roughness value for the GGX normal distribution function, D . The diffuse

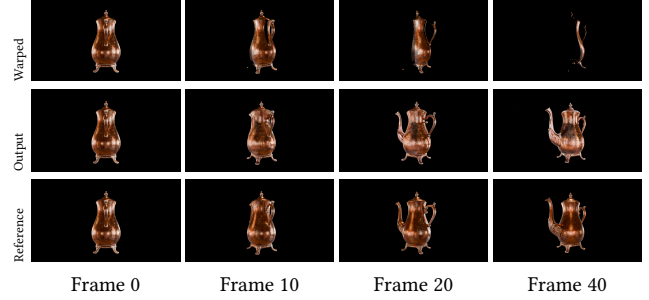


Fig. 4. Our image-to-material pipeline is conditioned on a single image, warped using a depth map to align with the current camera pose. The warping introduces disocclusion artifacts and incorrectly attaches specular highlights to the surface. The video model successfully inpaints the missing regions and generates plausible specular highlights

albedo is given by $k_d = c_{\text{base}} \cdot (1 - m)$, and specular albedo $k_s = 0.04 \cdot (1 - m) + c_{\text{base}} \cdot m$ [Karis 2013].

The rendering equation is evaluated using Monte Carlo integration, and we apply *multiple importance sampling* [Veach 1998], to reduce variance. We use three sampling techniques: light importance sampling [Pharr et al. 2023], cosine sampling for the diffuse lobe, and GGX importance sampling [Heitz 2018] for the specular lobe.

Optimization task. Let ϕ denote our optimization parameters (i.e., spatially varying material maps). For a given camera pose, c , the differentiable renderer produces an image $I_\phi(c)$. The reference image $I_{\text{ref}}(c)$ is a view from the same camera, generated by Video Model I. Given a loss function L , we minimize the empirical risk

$$\underset{\phi}{\operatorname{argmin}} \mathbb{E}_c [L(I_\phi(c), I_{\text{ref}}(c))] \quad (3)$$

using Adam [Kingma and Ba 2017] based on gradients w.r.t. the optimization parameters, $\partial L / \partial \phi$.

Our image loss, L_{image} , is L_1 norm on tonemapped and gamma corrected sRGB colors [Munkberg et al. 2022]. This is combined with a *scale invariant* regularizer loss:

$$L_{\text{reg}} = L_1(x/\bar{x}, y/\bar{y}), \quad (4)$$

applied to each of the predicted intrinsics (base color, roughness, metallic) from Video Model II, where we divide each image by its mean value before computing L_1 loss. The scale invariant formulation is more robust against biases in the predicted intrinsics. All loss terms are masked, applied only to pixels covered by the object. Our total loss function is $L = L_{\text{image}} + \lambda L_{\text{reg}}$. We use $\lambda = 0.2$ for all three regularizer terms, which empirically works well over our set of test scenes. We also experimented with adding an LPIPS [Zhang et al. 2018] loss term, but did not see improved results.

3.4 Image-conditioned Video Generation

While our primary focus is on material generation from text, our pipeline can also accommodate material generation from an image example since the Cosmos base model inherently supports both text and image conditioning. We adopt an approach similar to Gen3C [Ren et al. 2025] where the video model is conditioned



Fig. 5. Text-to-material generation. We compare against Paint-it [Youwang et al. 2024] and DreamMat [Zhang et al. 2024a] on three example meshes from the BlenderVault [Litman et al. 2025] dataset. We encourage the reader to compare the quality of the intrinsics (base color, roughness, metallic) to the reference. While significant deviations are expected in purely text-guided methods, we note that the base color predicted by our method is significantly more demodulated, or “flat” than the competing work. This is particularly noticeable for the GRAMOPHONE model. Our roughness and metallic guides are also more faithful to the reference, though with a slight bias towards lower roughness.

on an input image, which is warped (using a provided depth buffer) according to the camera trajectory. Please refer to Figure 4 for an example. As in our text-to-video setting, we additionally condition the video model on normals and three shading conditions. As described in Section 3.1 we start from the Cosmos [2025] model, and increase the input feature count of the input embedding layer of the diffusion model to account for our additional inputs (*warped image*, normals, and simple shading) and finetune the video model using our custom dataset. The reference image needs to (ideally) respect shape and lighting conditions of the additional inputs. We only tried this setting, and have not ablated the robustness of an arbitrary reference image.

4 RESULTS

We evaluate the quality of our results primarily against Paint-it [Youwang et al. 2024] and DreamMat [Zhang et al. 2024a], which use image diffusion models and score distillation sampling [Poole et al. 2022] for text-guided PBR material generation for a given 3D model. Paint-it re-parameterizes material textures as network weights of a U-Net, to regularize the noisy SDS-loss. We picked it as a representative comparison, as they compare favorably to recent SDS-based methods for texture and material generation [Chen et al. 2023b,a;

Richardson et al. 2023]. DreamMat finetunes an image diffusion model to condition on geometry and lighting and generates shaded views of an object with the same lighting. This disentangles lighting and appearance and improves PBR material quality. This is closely related to our approach, with the main differences being that we leverage video diffusion models for multi-view generation and material priors. We additionally compare to Make-it-Real [Fang et al. 2024], as a representative method retrieving materials from a database. We initialize Make-it-Real from the base color generated by DreamMat. The visual results are similar to DreamMat, and are left out for brevity. Please refer to Table 1 and our supplemental material for the full comparison.

In text-to-material applications, the reference is not clearly defined. To compute quantitative metrics, we took the following approach: We selected six 3D models with PBR materials from BlenderVault (held out from our training set), rendered out reference videos and generate captions for each example with CogVLM2 [Hong et al. 2024]. The generated prompts (see supplemental) and geometry for each model are used as input in our text-to-material evaluations. We use these six 3D models as ground truth when computing metrics for intrinsics and relighting evaluations.



Fig. 6. The HELMET model rendered with four light probes chosen to stress-test different lighting conditions. Our result show accurate specular reflections. DreamMat reproduces the global color tone of the probe, but the baked highlights are static and do not reflect the primary light direction.

PSNR (dB) \uparrow	relit	k_d	r	m	LPIPS \downarrow	relit	k_d
Our	20.1	20.1	16.9	14.1	Our	0.15	0.18
DreamMat	16.1	16.7	13.1	13.1	DreamMat	0.21	0.23
Make-it-Real	17.3	16.7	17.5	13.2	Make-it-Real	0.20	0.23
Paint-it	14.0	13.8	14.1	10.0	Paint-it	0.22	0.26

Table 1. Image metrics for text-to-materials methods. Each material is compared to a reference 3D model from which we generated the prompt and used the geometry. Scores for intrinsics are averaged over six test scenes, and relighting results are averaged over six test scenes, each scene lit with eight light probes.

Figure 5 shows qualitative results. We note that our method outperforms previous work in terms of intrinsics and relighting quality. This is apparent in the base color of the GRAMOPHONE scene, where our method produces a demodulated texture, similar to the reference, while the base color produced by Paint-it and DreamMat both show baked specular highlights. Similar behavior is also clearly noticeable in the DIVER and SHOES examples. Our roughness and metallic guides are noisy, and somewhat biased towards lower roughness (more specular reflections). However, they are considerably more faithful to the reference than the competing methods. Please refer to the supplement for additional scenes and videos.

In Figure 6, we relight the extracted materials with four different probes. DreamMat captures the overall color tone of each probe, but the baked highlights make the lighting appear to always come from the same direction. This is apparent in the *Grace Cathedral* probe, where the main light source is placed straight above the object. We present error metrics in Table 1. Considering base color and relighting results, we note that our method scores highest or on par with the competing methods for all scenes. As an outlier, we score



Fig. 7. Our finetuned video model generates view-consistent multi-view images of diverse materials from text prompts, while closely respecting the input geometry and lighting.

lower than DreamMat on the roughness and metallic guides for the SHED scene (see supplement), which is explained by our method adding metallic features, which, while plausible, are not present in the reference example.

4.1 User study

To evaluate the perceptual quality of the generated texture and materials, we conducted a user study where participants were presented with paired video rendering in random order—one generated by our method and the other by a baseline method. Participants were asked to compare the two results, assess the quality of texture and material realism, and choose the image they perceived as more visually appealing.

We render each asset with four different lighting conditions, resulting in a set of 24 samples to evaluate. We invite 11 users to make a binary selection for each video pair, and then apply majority voting to determine the preferred method for each video sample.

Additionally, inspired by recent work on using VLMs as perceptual evaluators [Wu et al. 2024b], we randomly sample seven frames per video and conduct the same evaluation on image pairs using GPT-4o [OpenAI 2024] as the perceptual evaluator. In Table 2, we report the percentage of samples where our method was preferred over the baselines. The average user preference for our method is above 50% for both human and VLM evaluators, showing our method outperforms baselines with higher perceptual quality.

Setting	Human Eval.	VLM Eval.
Our over DreamMat [Zhang et al. 2024a]	62%	62%
Our over Paint-it [Youwang et al. 2024]	58%	100%

Table 2. **User study.** We report the percentage of samples where our method is preferred over baselines, based on evaluations from both human annotators and a VLM (GPT-4o). A preference score above 50% indicates that our method is favored.

4.2 Ablations

Material diversity. Our finetuned video model leverages the powerful base model of Cosmos, and can generate a diverse set of materials. In Figure 7 we prompt the model with ten different material descriptions while keeping the lighting and geometry constant. The video model produces view-consistent, high-quality video frames, while respecting the input geometry and lighting.

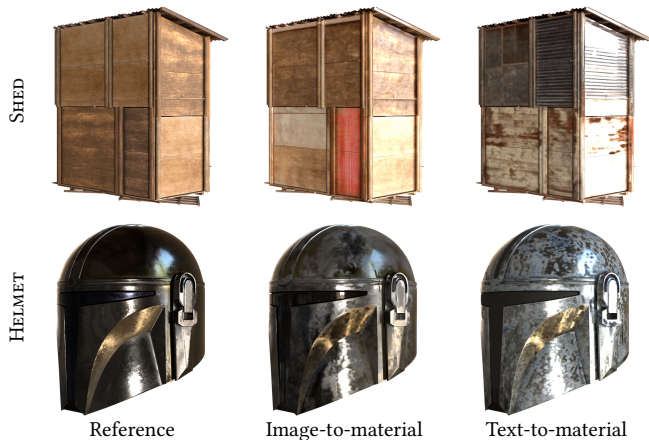


Fig. 8. Two examples comparing our text- and image-guided models. The image-to-material model is guided by a single shaded view from the reference scene, in addition to the text prompt, and consequently respects the aesthetics of the reference scene better.

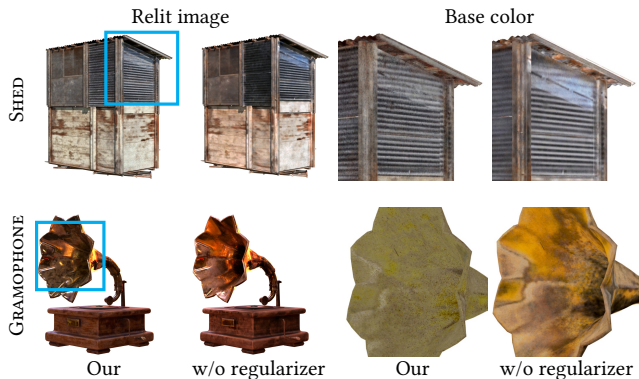


Fig. 9. The impact of using intrinsic guides for regularization. Differentiable rendering sometimes struggles with disentangling lighting from materials. Without regularizer, the strong shadow from the roof is not demodulated in the SHED scene. Similarly, the GRAMOPHONE example exhibits clear base color darkening in the horn, which creates an overly shadowed region when lit.

Image-conditioning. We evaluate our image-conditioned video model by providing a single rendered view of the reference 3D model in addition to the text prompt, effectively performing material inpainting. As expected, Figure 8 shows that the resulting materials match the style of the reference more closely, and this is also reflected in the errors metrics below.

PSNR \uparrow	relit	k_d	r	m	LPIPS \downarrow	relit	k_d
Our-text	20.1	20.1	17.0	14.1	Our-text	0.15	0.18
Our-image	21.1	21.0	17.1	15.4	Our-image	0.13	0.15

Impact of regularization with intrinsics. We ablate the intrinsic regularization in Figure 9. While multi-view reconstruction from the generated video frames with our differentiable path tracer works reasonably well, we note that the intrinsic guides help demodulate the albedo, and reduce discontinuities in metallic and roughness

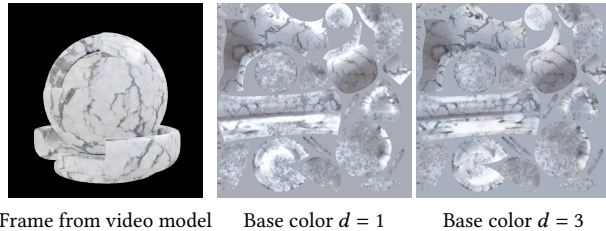


Fig. 10. Impact of physically-based rendering. In this example, a significant portion of the lighting comes from indirect bounces. We visualize the reconstructions from differentiable path tracing with one ($d = 1$) vs. three bounces ($d = 3$). By more accurately simulating global illumination, we obtain a more uniform base color with less baked lighting.

parameters, resulting in a more natural look. This is further corroborated by a small but significant quality improvement, as shown in the metrics below.

PSNR \uparrow	relit	k_d	r	m	LPIPS \downarrow	relit	k_d
Our	20.1	20.1	17.0	14.1	Our	0.15	0.18
No reg.	19.2	18.6	18.5	12.8	No reg.	0.16	0.18

Impact of differentiable path tracing. The base video model we leverage is trained on natural images and captured videos. To reduce the domain gap between computer generated images and photographs, we opted for physically-based rendering with path tracing, incorporating reflections, shadows, and global illumination effects, both when generating our training data and for inverse rendering. Path tracing is more expensive and introduce higher noise level due to extensive use of Monte Carlo integration to approximate lighting. However, it produces more realistic images and helps disentangle lighting from material parameters. Figure 10 is an illustrative example of reduced light baking by more accurate simulation of multiple light bounces.

5 CONCLUSION AND LIMITATIONS

We conclude that modern video diffusion models combined with high-quality differentiable rendering show great promise for text-guided PBR material generation. While we limit ourselves to material generation, we believe our method can be a valuable component in larger systems targeting text-to-3D, single-image reconstruction, and for material augmentation for 3D datasets.

A limitation of our current prototype is multi-view coverage. The base model we leverage expects smooth camera movements, and we use 360° orbits with a fixed elevation. Unseen areas of the mesh will not be accurately reconstructed, and textures will contain data extrapolated by the hash grid+MLP [Müller et al. 2022] representation. Ideally, we would like to uniformly distribute our views on a sphere around the object to maximize coverage. Recent works [Gao* et al. 2024; Wu et al. 2024a] show promising signs of this type of camera control, but the models are currently not publicly available.

Furthermore, current video models target natural videos and use aggressively compressed latent spaces, which shows up in generated videos as motion blur and video compression artifacts. This breaks the pinhole camera and instant shutter assumptions of our

differentiable renderer. Optimization with an L_1 loss recovers some image detail, but that a more principled solution is desired to reduce blur. We are hopeful that our method will greatly benefit from future video models, which is a very active research field.

We currently do not consider normal mapping and rely on geometric normals for shading. Normal mapping can be trivially enabled in our differentiable renderer, and DiffusionRenderer outputs a normal intrinsics map, but we note that previous work struggles with the fundamentally under-determined problem of normal map optimization [Munkberg et al. 2022]. Robust priors, or regularizers, would be required for high quality results, and we leave this to future work.

An interesting avenue for future work is to leverage image-conditioned models (Section 3.4), to generate localized coverage and slow down camera movement, by stitching together multiple videos. We would also like to expand the material extraction to handle more rendering effects, e.g., refractions and subsurface scattering. While our early experiments are encouraging, these experiments require novel datasets.

ACKNOWLEDGMENTS

The authors are grateful to Aaron Lefohn, Sanja Fidler, Ming-Yu Liu, and Jun Gao for their support and discussions during this research, as well as the anonymous reviewers for their valuable comments and feedback.

REFERENCES

- Sai Praveen Bangaru, Lifan Wu, Tzu-Mao Li, Jacob Munkberg, Gilbert Bernstein, Jonathan Ragan-Kelley, Frédo Durand, Aaron Lefohn, and Yong He. 2023. SLANG.D: Fast, Modular and Differentiable Shader Programming. *ACM Trans. Graph.* 42, 6, Article 264 (2023).
- Andreas Blattmann, Tim Dockhorn, Sumith Kulal, Daniel Mendelevitch, Maciej Kilian, Dominik Lorenz, Yam Levi, Zion English, Vikram Voleti, Adam Letts, Varun Jampani, and Robin Rombach. 2023a. Stable Video Diffusion: Scaling Latent Video Diffusion Models to Large Datasets. *arXiv:2311.15127* (2023).
- Andreas Blattmann, Robin Rombach, Huan Ling, Tim Dockhorn, Seung Wook Kim, Sanja Fidler, and Karsten Kreis. 2023b. Align your Latents: High-Resolution Video Synthesis with Latent Diffusion Models. In *IEEE Conference on Computer Vision and Pattern Recognition (CVPR)*.
- Brent Burley. 2012. Physically Based Shading at Disney. In *SIGGRAPH Courses: Practical Physically Based Shading in Film and Game Production*.
- Duygu Ceylan, Valentin Deschaintre, Thibault Groueix, Rosalie Martin, Chun-Hao Huang, Romain Rouffet, Vladimir Kim, and Gaëtan Lussagne. 2024. MatAtlas: Text-driven Consistent Geometry Texturing and Material Assignment. *arXiv:2404.02899* <https://arxiv.org/abs/2404.02899>
- Dave Zhenyu Chen, Yawar Siddiqui, Hsin-Ying Lee, Sergey Tulyakov, and Matthias Nießner. 2023b. Text2tex: Text-driven texture synthesis via diffusion models. In *Proceedings of the IEEE/CVF international conference on computer vision*. 18558–18568.
- Rui Chen, Yongwei Chen, Ningxin Jiao, and Kui Jia. 2023a. Fantasia3D: Disentangling Geometry and Appearance for High-quality Text-to-3D Content Creation. In *Proceedings of the IEEE/CVF International Conference on Computer Vision (ICCV)*. 22246–22256.
- Zhaoxi Chen, Jiayang Tang, Yuhao Dong, Ziang Cao, Fangzhou Hong, Yushi Lan, Tengfei Wang, Haozhe Xie, Tong Wu, Shunsuke Saito, Liang Pan, Dahua Lin, and Ziwei Liu. 2024. 3DTopia-XL: High-Quality 3D PBR Asset Generation via Primitive Diffusion. *arXiv preprint arXiv:2409.12957* (2024).
- Jasmine Collins, Shubham Goel, Kenan Deng, Achleshwar Luthra, Leon Xu, Erhan Gundogdu, Xi Zhang, Tomas F Yago Vicente, Thomas Dideriksen, Himanshu Arora, Matthieu Guillaumin, and Jitendra Malik. 2022. ABO: Dataset and Benchmarks for Real-World 3D Object Understanding. *CVPR* (2022).
- Robert L. Cook and Kenneth E. Torrance. 1982. A reflectance model for computer graphics. *ACM Transactions on Graphics (TOG)* 1, 1 (1982), 7–24.
- Matt Deitke, Dustin Schwenk, Jordi Salvador, Luca Weihs, Oscar Michel, Eli Vander-Bilt, Ludwig Schmidt, Kiana Ehsani, Aniruddha Kembhavi, and Ali Farhadi. 2023. Objaverse: A Universe of Annotated 3D Objects. In *Proceedings of the IEEE/CVF Conference on Computer Vision and Pattern Recognition*. 13142–13153.
- Kangle Deng, Timothy Omernick, Alexander Weiss, Deva Ramanan, Jun-Yan Zhu, Tinghui Zhou, and Maneesh Agrawala. 2024. FlashTex: Fast Relightable Mesh Texturing with LightControlNet. In *European Conference on Computer Vision (ECCV)*.
- Prafulla Dhariwal and Alexander Quinn Nichol. 2021. Diffusion Models Beat GANs on Image Synthesis. In *Advances in Neural Information Processing Systems*.
- Ye Fang, Zeyi Sun, Tong Wu, Jiaqi Wang, Ziwei Liu, Gordon Wetzstein, and Dahua Lin. 2024. Make-it-Real: Unleashing Large Multimodal Model for Painting 3D Objects with Realistic Materials. *arXiv:2404.16829* [cs.CV]
- Ruiqi Gao*, Aleksander Holynski*, Philipp Henzler, Arthur Brussee, Ricardo Martin-Brualla, Pratul P. Srinivasan, Jonathan T. Barron, and Ben Poole*. 2024. CAT3D: Create Anything in 3D with Multi-View Diffusion Models. *Advances in Neural Information Processing Systems* (2024).
- Eric Heitz. 2018. Sampling the GGX Distribution of Visible Normals. *Journal of Computer Graphics Techniques (JCGT)* 7, 4 (2018), 1–13.
- Jonathan Ho, Ajay Jain, and Pieter Abbeel. 2020. Denoising diffusion probabilistic models. *Advances in Neural Information Processing Systems* 33 (2020), 6840–6851.
- Wenyi Hong, Ming Ding, Wendi Zheng, Xinghan Liu, and Jie Tang. 2023. CogVideo: Large-scale Pretraining for Text-to-Video Generation via Transformers. In *The Eleventh International Conference on Learning Representations*.
- Wenyi Hong, Weihang Wang, Ming Ding, Wenmeng Yu, Qingsong Lv, Yan Wang, Yean Cheng, Shiyu Huang, Junhui Ji, Zhao Xue, et al. 2024. CogVLM2: Visual Language Models for Image and Video Understanding. *arXiv preprint arXiv:2408.16500* (2024).
- Wenzel Jakob, Sébastien Speierer, Nicolas Roussel, Merlin Nimier-David, Delio Vicini, Tizian Zeltner, Baptiste Nicolet, Miguel Crespo, Vincent Leroy, and Ziyi Zhang. 2022. Mitsuba 3 renderer. <https://mitsuba-renderer.org>.
- Haian Jin, Yuan Li, Fujun Luan, Yuanbo Xiangli, Sai Bi, Kai Zhang, Zexiang Xu, Jin Sun, and Noah Snavely. 2024. Neural Gaffer: Relighting Any Object via Diffusion. In *Advances in Neural Information Processing Systems*.
- James T. Kajiya. 1986. The rendering equation. In *Proceedings of the 13th Annual Conference on Computer Graphics and Interactive Techniques*. 143–150.
- Brian Karis. 2013. Real shading in Unreal Engine 4. *ACM SIGGRAPH Course on Physically Based Shading Theory and Practice* 4, 3 (2013), 1.
- Bernhard Kerbl, Georgios Kopanas, Thomas Leimkühler, and George Drettakis. 2023. 3D Gaussian Splatting for Real-Time Radiance Field Rendering. *ACM Transactions on Graphics* 42, 4 (July 2023). <https://repo-sam.inria.fr/fungraph/3d-gaussian-splatting/>
- Mukul Khanna*, Yongsun Mao*, Hanxiao Jiang, Sanjay Haresh, Brennan Shacklett, Dhruv Batra, Alexander Clegg, Eric Undersander, Angel X. Chang, and Manolis Savva. 2023. Habitat Synthetic Scenes Dataset (HSSD-200): An Analysis of 3D Scene Scale and Realism Tradeoffs for ObjectGoal Navigation. *arXiv preprint* (2023). *arXiv:2306.11290* [cs.CV]
- Diederik P. Kingma and Jimmy Ba. 2017. Adam: A Method for Stochastic Optimization. *arXiv:1412.6980* [cs.LG]
- Peter Kocsis, Lukas Höllein, and Matthias Nießner. 2025. IntrinsicX: High-Quality PBR Generation using Image Priors. *arXiv:2504.01008* [cs.CV]
- Samuli Laine, Janne Hellsten, Tero Karras, Yeongho Seol, Jaakko Lehtinen, and Timo Aila. 2020. Modular Primitives for High-Performance Differentiable Rendering. *ACM Transactions on Graphics* 39, 6 (2020).
- Ruofan Liang, Zan Gojcic, Huan Ling, Jacob Munkberg, Jon Hasselgren, Zhi-Hao Lin, Jun Gao, Alexander Keller, Nandita Vijaykumar, Sanja Fidler, and Zian Wang. 2025. DiffusionRenderer: Neural Inverse and Forward Rendering with Video Diffusion Models. In *Proceedings of the IEEE/CVF Conference on Computer Vision and Pattern Recognition*.
- Yehonathan Litman, Or Patashnik, Kangle Deng, Aviral Agrawal, Rushikesh Zawat, Fernando De la Torre, and Shubham Tulsiani. 2025. MaterialFusion: Enhancing Inverse Rendering with Material Diffusion Priors. In *3DV*.
- André Mazzone and Chris Rydalch. 2023. Standard Shader Ball: A Modern and Feature-Rich Render Test Scene. In *SIGGRAPH Asia 2023 Technical Communications (SA '23)*. Article 14, 3 pages.
- Ben Mildenhall, Pratul P. Srinivasan, Matthew Tancik, Jonathan T. Barron, Ravi Ramamoorthi, and Ren Ng. 2020. NeRF: Representing Scenes as Neural Radiance Fields for View Synthesis. In *ECCV*.
- Thomas Müller, Alex Evans, Christoph Schied, and Alexander Keller. 2022. Instant Neural Graphics Primitives with a Multiresolution Hash Encoding. *ACM Trans. Graph.* 41, 4 (2022), 102:1–102:15.
- Jacob Munkberg, Jon Hasselgren, Tianchang Shen, Jun Gao, Wenzheng Chen, Alex Evans, Thomas Müller, and Sanja Fidler. 2022. Extracting Triangular 3D Models, Materials, and Lighting From Images. In *Proceedings of the IEEE/CVF Conference on Computer Vision and Pattern Recognition (CVPR)*. 8280–8290.
- NVIDIA. 2025. Cosmos World Foundation Model Platform for Physical AI. *arXiv preprint arXiv:2501.03575* (2025).
- OpenAI. 2024. GPT-4o System Card. *arXiv:2410.21276* <https://arxiv.org/abs/2410.21276>
- Steven G. Parker, James Bigler, Andreas Dietrich, Heiko Friedrich, Jared Hoberock, David Luebke, David McAllister, Morgan McGuire, Keith Morley, Austin Robison, and Martin Stich. 2010. OptiX: A general purpose ray tracing engine. *ACM Trans. Graph.* 29, 4, Article 66 (2010), 13 pages.
- Matt Pharr, Wenzel Jakob, and Greg Humphreys. 2023. *Physically Based Rendering - From Theory to Implementation*. Morgan Kaufmann, fourth edition.

- Ben Poole, Ajay Jain, Jonathan T. Barron, and Ben Mildenhall. 2022. DreamFusion: Text-to-3D using 2D Diffusion. *arXiv* (2022).
- Xuanchi Ren, Tianchang Shen, Jiahui Huang, Huan Ling, Yifan Lu, Merlin Nimier-David, Thomas Müller, Alexander Keller, Sanja Fidler, and Jun Gao. 2025. GEN3C: 3D-Informed World-Consistent Video Generation with Precise Camera Control. In *Proceedings of the IEEE/CVF Conference on Computer Vision and Pattern Recognition*.
- Elad Richardson, Gal Metzer, Yuval Alaluf, Raja Giryes, and Daniel Cohen-Or. 2023. TEXTure: Text-guided texturing of 3d shapes. In *ACM SIGGRAPH 2023 conference proceedings*. 1–11.
- Nataniel Ruiz, Yuanzhen Li, Varun Jampani, Yael Pritch, Michael Rubinstein, and Kfir Aberman. 2022. DreamBooth: Fine Tuning Text-to-image Diffusion Models for Subject-Driven Generation. *arXiv preprint arxiv:2208.12242* (2022).
- Yichun Shi, Peng Wang, Jianglong Ye, Long Mai, Kejie Li, and Xiao Yang. 2023. MV-Dream: Multi-view Diffusion for 3D Generation. *arXiv:2308.16512* (2023).
- Jascha Sohl-Dickstein, Eric Weiss, Niru Maheswaranathan, and Surya Ganguli. 2015. Deep Unsupervised Learning Using Nonequilibrium Thermodynamics. In *International Conference on Machine Learning*.
- Eric Veach. 1998. *Robust Monte Carlo methods for light transport simulation*. Stanford University.
- Vikram Voleti, Chun-Han Yao, Mark Boss, Adam Letts, David Pankratz, Dmitrii Tochilkin, Christian Laforte, Robin Rombach, and Varun Jampani. 2024. SV3D: Novel Multi-view Synthesis and 3D Generation from a Single Image using Latent Video Diffusion. In *European Conference on Computer Vision (ECCV)*.
- Bruce Walter, Stephen R. Marschner, Hongsong Li, and Kenneth E. Torrance. 2007. Microfacet Models for Refraction through Rough Surfaces. In *Proceedings of the 18th Eurographics Conference on Rendering Techniques*. 195–206.
- Zhengyi Wang, Cheng Lu, Yikai Wang, Fan Bao, Chongxuan Li, Hang Su, and Jun Zhu. 2023. ProlificDreamer: High-Fidelity and Diverse Text-to-3D Generation with Variational Score Distillation. In *Advances in Neural Information Processing Systems (NeurIPS)*.
- Rundi Wu, Ruiqi Gao, Ben Poole, Alex Trevithick, Changxi Zheng, Jonathan T. Barron, and Aleksander Holynski. 2024a. CAT4D: Create Anything in 4D with Multi-View Video Diffusion Models. *arXiv:2411.18613* (2024).
- Tong Wu, Guandao Yang, Zhibing Li, Kai Zhang, Ziwei Liu, Leonidas Guibas, Dahua Lin, and Gordon Wetzstein. 2024b. GPT-4V(ision) is a Human-Aligned Evaluator for Text-to-3D Generation. In *CVPR*.
- Chen Xi, Peng Sida, Yang Dongchen, Liu Yuan, Pan Bowen, Lv Chengfei, and Zhou Xiaowei. 2024. IntrinsicAnything: Learning Diffusion Priors for Inverse Rendering Under Unknown Illumination. *arxiv: 2404.11593* (2024).
- Jianfeng Xiang, Zelong Lv, Sicheng Xu, Yu Deng, Ruicheng Wang, Bowen Zhang, Dong Chen, Xin Tong, and Jialong Yang. 2024. Structured 3D Latents for Scalable and Versatile 3D Generation. *arXiv preprint arXiv:2412.01506* (2024).
- Haibo Yang, Yang Chen, Yingwei Pan, Ting Yao, Zhineng Chen, Chong-Wah Ngo, and Tao Mei. 2024a. Hi3D: Pursuing High-Resolution Image-to-3D Generation with Video Diffusion Models. In *ACM MM*.
- Zhuoyi Yang, Jiayan Teng, Wendi Zheng, Ming Ding, Shiyu Huang, Jiazheng Xu, Yuanming Yang, Wenyi Hong, Xiaohan Zhang, Guanyu Feng, Da Yin, Xiaotao Gu, Yuxuan Zhang, Weihao Wang, Yean Cheng, Ting Liu, Bin Xu, Yuxiao Dong, and Jie Tang. 2024b. CogVideoX: Text-to-Video Diffusion Models with An Expert Transformer.
- Yu-Ying Yeh, Jia-Bin Huang, Changil Kim, Lei Xiao, Thu Nguyen-Phuoc, Numair Khan, Cheng Zhang, Manmohan Chandraker, Carl S Marshall, Zhao Dong, et al. 2024. TextureDreamer: Image-guided Texture Synthesis through Geometry-aware Diffusion. *arXiv preprint arXiv:2401.09416* (2024).
- Kim Youwang, Tae-Hyun Oh, and Gerard Pons-Moll. 2024. Paint-it: Text-to-Texture Synthesis via Deep Convolutional Texture Map Optimization and Physically-Based Rendering. In *IEEE Conference on Computer Vision and Pattern Recognition (CVPR)*.
- Xin Yu, Ze Yuan, Yuan-Chen Guo, Ying-Tian Liu, Jianhui Liu, Yangguang Li, Yan-Pei Cao, Ding Liang, and Xiaojuan Qi. 2024. TEXGen: a Generative Diffusion Model for Mesh Textures. *ACM Trans. Graph.* 43, 6, Article 213 (2024).
- Greg Zaal and et al. 2024. *Poly Haven - The Public 3D Asset Library*. <https://polyhaven.com>
- Chong Zeng, Yue Dong, Pieter Peers, Youkang Kong, Hongzhi Wu, and Xin Tong. 2024c. DiLightNet: Fine-grained Lighting Control for Diffusion-based Image Generation. In *ACM SIGGRAPH 2024 Conference Papers*.
- Xianfang Zeng, Xin Chen, Zhongqi Qi, Wen Liu, Zibo Zhao, Zhibin Wang, Bin Fu, Yong Liu, and Gang Yu. 2024a. Paint3d: Paint anything 3d with lighting-less texture diffusion models. In *Proceedings of the IEEE/CVF conference on computer vision and pattern recognition*. 4252–4262.
- Zheng Zeng, Valentin Deschaintre, Iliyan Georgiev, Yannick Hold-Geoffroy, Yiwei Hu, Fujun Luan, Ling-Qi Yan, and Miloš Hašan. 2024b. RGB \leftrightarrow X: Image decomposition and synthesis using material-and lighting-aware diffusion models. In *ACM SIGGRAPH 2024 Conference Papers*. 1–11.
- Cheng Zhang, Bailey Miller, Kai Yan, Ioannis Gkioulekas, and Shuang Zhao. 2020. Path-Space Differentiable Rendering. *ACM Trans. Graph.* 39, 4 (2020), 143:1–143:19.
- Longwen Zhang, Ziyu Wang, Qixuan Zhang, Qiwei Qiu, Anqi Pang, Haoran Jiang, Wei Yang, Lan Xu, and Jingyi Yu. 2024c. CLAY: A Controllable Large-scale Generative Model for Creating High-quality 3D Assets. *ACM Transactions on Graphics (TOG)* 43, 4 (2024), 1–20.
- Richard Zhang, Phillip Isola, Alexei A. Efros, Eli Shechtman, and Oliver Wang. 2018. The unreasonable effectiveness of deep features as a perceptual metric. In *Proceedings of the IEEE conference on computer vision and pattern recognition*. 586–595.
- Shangzhan Zhang, Sida Peng, Tao Xu, Yuanbo Yang, Tianrun Chen, Nan Xue, Yujun Shen, Hujun Bao, Ruizhen Hu, and Xiaowei Zhou. 2024b. MaPa: Text-driven Photorealistic Material Painting for 3D Shapes. In *ACM SIGGRAPH 2024 Conference Papers*. Article 4, 12 pages.
- Yuqing Zhang, Yuan Liu, Zhiyu Xie, Lei Yang, Zhongyuan Liu, Mengzhou Yang, Runze Zhang, Qilong Kou, Cheng Lin, Wenping Wang, and Xiaogang Jin. 2024a. DreamMat: High-quality PBR Material Generation with Geometry- and Light-aware Diffusion Models. *ACM Trans. Graph.* 43, 4, Article 39 (2024).
- Xiaoming Zhao, Pratul P. Srinivasan, Dor Verbin, Keunhong Park, Ricardo Martin Brualla, and Philipp Henzler. 2024. IllumiNeRF: 3D Relighting Without Inverse Rendering. In *NeurIPS*.
- Junzhe Zhu and Peiye Zhuang. 2023. HiFA: High-fidelity Text-to-3D Generation with Advanced Diffusion Guidance. *arXiv:2305.18766* [cs.CV]
- Shenhao Zhu, Lingteng Qiu, Xiaodong Gu, Zhengyi Zhao, Chao Xu, Yuxiao He, Zhe Li, Xiaoguang Han, Yao Yao, Xun Cao, Siyu Zhu, Weihao Yuan, Zilong Dong, and Hao Zhu. 2024. MCMat: Multiview-Consistent and Physically Accurate PBR Material Generation.